Multidiszciplináris Tudományok, 15. kötet, 3. sz. (2025) pp. 90–97. ***https://doi.org/10.35925/j.multi.2025.3.9***

ON THE INSTABILITY OF TWO- AND THREE-PINNED CIRCULAR ARCHES

László Péter Kiss
associate professor, Institute of Applied Mechanics
3515 Miskolc-Egyetemváros, e-mail: mechkiss@uni-miskolc.hu

Muhammad Hamza Daud
MSc student, Institute of Machine Tools and Mechatronics
3515 Miskolc-Egyetemváros, e-mail: hamzadaud1100@gmail.com

Abstract

Arches are important building blocks that are known for their ability to efficiently distribute loads. That is why they are widely studied. The two-pinned arc has hinges at each end that allow rotation but prevent translation. When loaded on the axis of symmetry, it creates bending moments besides internal forces that affect the stability. The three-pinned arch has an extra inner hinge, this time, at the crown. This hinge allows the moment to relax. However, the inner hinge can introduce additional modes of deformation. Two- and three-pinned slender, circular arches are compared within this work to find out the lowest buckling loads, displacements and inner forces. The external load acts on the axis of symmetry. The span is a fixed value and arches with different angles are placed between the end-supports, starting from very flat (almost straight) to deep geometries. From the selected perspective, it is found that two-pinned arches are stiffer throughout the whole investigated domain. The novel model is also compared with finite element computations and a good correlation can be found.

Keywords: *arch, buckling, three-pinned, nonlinear*

1. Introduction

Arches are important building blocks that are known for their ability to efficiently distribute loads. Two- and three-pinned arches have been widely studied for their positive stability properties. The two-pinned arc has hinges at each end that allow rotation but prevent translation. This system is statically indeterminate and is commonly used in structural applications. When loaded on the axis of symmetry, it creates bending moments besides internal forces that affect the stability. The three-pinned arch has an extra inner hinge at the crown. This hinge allows the moment to relax, redistributing the inner forces more effectively. However, the inner hinge can introduce additional modes of deformation. These arches react differently under symmetrical loads.

The number of open literature results is numerous regarding arches. The reader is referred to the likes of (Simitses, 1976; Bazant and Cedolin, 2010; Gönczi and Ecsedi, 2022; Ecsedi et al., 2023). Furthermore, it is mentioned that publication (Dawe, 1974a) focuses on both deep and shallow arches, testing multiple strain-displacement assumptions for their buckling. An improved buckling theory is given in (Dave, 1974b) by the same author. Large displacements and rotations are assumed in (Gummadi and Palazotto, 1997; Palazotto et al., 1997) and five models are compared for the stability of straight and curved beams. Furthermore, article (Bateni and Eslami, 2014) deals with functionally graded

materials. The loading is a concentrated force in the stability investigations of (Bradford et al., 2008; Yan et al., 2017; Yan et al., 2018), while it is evenly distributed in (Bradford et al., 2002). Within these sources, the end-support conditions are also varying.

The literature on arches with an internal pin is much more limited compared to continuous ones. Nevertheless, these structures are still favoured for two main reasons (Karnovky and Lebed, 2021). They allow for large spans composed of not one but two structural parts, and the internal hinge prevents the transfer of moments. Typically, the internal hinge is located at the crown point, although its position can vary based on factors like different ground level at the ends. Article (Pi and Bradford, 2015) studies elastic three-hinged arches analytically, while (Kiss, 2024) is about fixed-pinned-fixed arches. Similar research in (Pi and Bradford, 2014) explores uniform radial loads and temperature effects. Paper (Oliveira et al., 2021) focuses on three-pinned arches, offering results obtained through commercial software and comprehensive studies on the impact of various parameters, such as geometry, material properties, and boundary conditions. Furthermore, in (Bradford and Pi, 2015), the attention is on crown-pinned concrete-filled steel tubular arches, with a long-term analysis that considers creep and shrinkage of the concrete core under a sustained concentrated load.

This study compares two- and three-pinned arches under a force acting on the axis of symmetry with the hypothesis of references (Kiss, 2024; Kiss, 2015). It focuses on critical loads, displacements and inner force distributions as main aspects.

2. Selected arch geometries, computational results

Figure 1 shows the initial configuration of the arches in question under the external load Q. The angle coordinate is ϕ, that is zero at the symmetry axis and is positive clockwise. The meaning of further notations are gathered in *Table 1*. The kinematical hypothesis and equilibrium equations can be found in details in [16, 20]. The material is linearly elastic. It is emphasised that moderately large rotations are considered that makes the problem nonlinear.

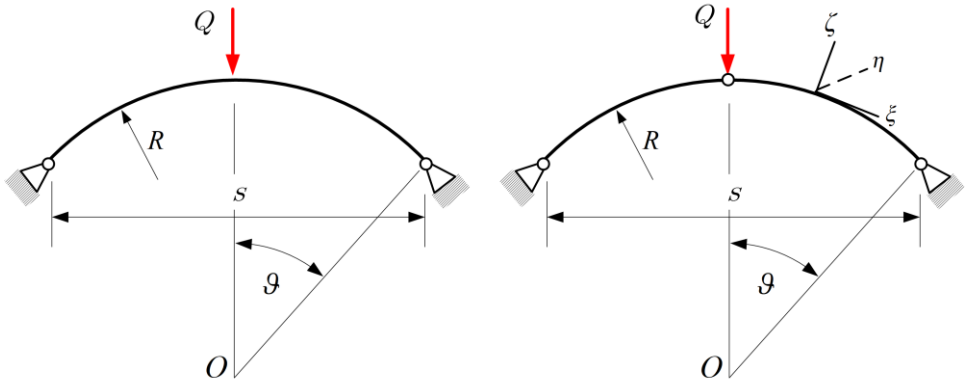

Figure 1. *(a) Two-; (b) three-pinned arch model*

The very first step before the evaluation of the results is the validation to find out whether our custom Maple code returns credible results. The tested geometrical and material data are gathered in *Table 1*. for rectangular section. It is assumed that the span (distance between the end supports) is given in advance. A very flat (almost straight), a shallow and a deep arch will be compared in this context from the mechanical behaviour perspective.

Table 1
Geometrical and material data

arch half angle	ϑ	[rad]	*0.1*	*0.4*	*1.2*
arch span	*s*	[mm]	*9735.5*	*9735.5*	*9735.5*
arch rise	*h*	[mm]	*244*	*986.74*	*3330.2*
arch length	*S*	[mm]	*9752*	*10000*	*12534*
arch radius	*R*	[mm]	*48759*	*12500*	*5223*
Young's modulus	*E*	[MPa]	*210000*	*210000*	*210000*
section width	*a*	[mm]	*50*	*50*	*50*
section height	*b*	[mm]	*100*	*100*	*100*
section area	*A*	[mm^2]	*5000*	*5000*	*5000*
strong axis inertia	*I*	[mm^4]	*4.17e6*	*4.17e6*	*4.17e6*
slenderness	*S/r*	[–]	*337.81*	*346.41*	*434.20*
rise to span	*h/s*	[–]	*0.025*	*0.1*	*0.34*

For the finite element (FE) computations, carried out with Abaqus, the geometry was mapped with 50 pcs. of B21 elements. In the contact point of the two-half arches, engineering constraint was assigned. When it is a two-pinned arch, the constraint type was Tie, and for three-pinned members, it was Pin type. The Static, Riks step was set up to trace the limit points on the equilibrium path. The initial concentrated load magnitude was set to unit. Comparison of the lowest critical loads can be made as per the results of Table 2, where the dimensionless load $P = QR^2 \vartheta/IE$. The findings coincide extremely well when $\vartheta = 0.1$ or 0.4. When $\vartheta = 1.2$, the discrepancy is a bit higher for the 3-pinned arch, suggesting the new model might not be that accurate for such (deep) arches.

Table 2
Comparison of the limit point loads with FE

arch half angle	ϑ	[rad]	*0.1*	*0.4*	*1.2*
3-pinned, new model	*P*	[–]	*1.16*	*1.32*	*1.76*
2-pinned, new model	*P*	[–]	*5.75*	*6.67*	*6.91*
3-pinned, FE	*P*	[–]	*1.16*	*1.28*	*1.40*
2-pinned, FE	*P*	[–]	*5.76*	*6.74*	*7.36*

As mentioned previously, the material, arch span and cross-section are fixed as listed in *Table 1*. Numerical evaluations are performed with these conditions – by changing the span/rise ratio through the arch angle.

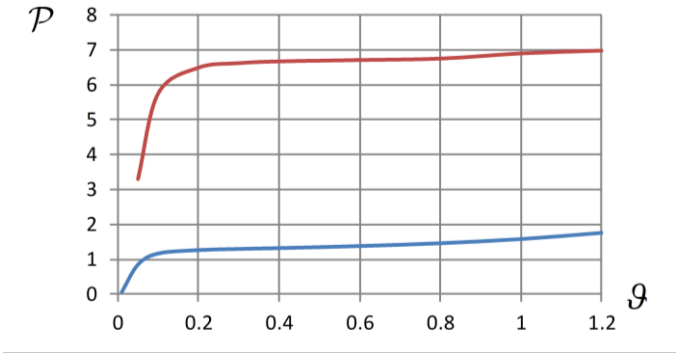

Figure 2. *Buckling load variation for two-pinned (red curve) and three-pinned (blue curve) arches*

Figure 2 compares the lowest limit-point dimensionless buckling loads against the semi-vertex angle of the arch. The blue curve represents the 3-pinned setup, and the red curve is valid for the 2-pinned member. The major findings:

- The buckling load is always greater for the 2-pinned arch.
- Buckling can occur from lower arch angles for the 3-pinned case.
- The curves begin with a steep part for lower arch angles.
- After a while, the curves become flat, meaning the buckling load is just slightly affected by the rise of the angle.
- The buckling load is at least 3.9 times greater for 2-pinned arches.
- The buckling load is at most 5.1 times greater for 2-pinned arches within the assessed domain.
-

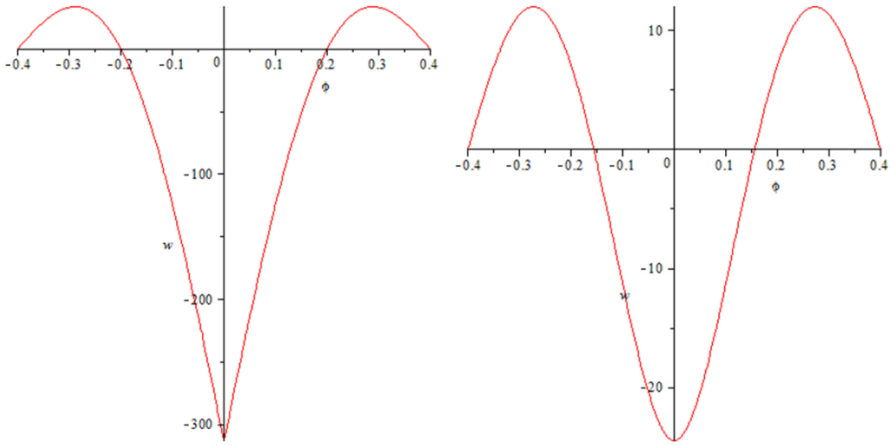

Figure 3. *ϑ = 0.4, (a) three-pinned,*
(b) two-pinned arch – normal displacement against the angle coordinate

In the sequel, the mechanical state of two- and three pinned arches are compared when $\vartheta = 0.4$ and the external load is the same, i.e., 99.999% of the load that causes the buckling of the three-pinned arch. This load level, therefore, is P = 1.3199 as per *Figure 1* and *Table 2*.

As it is already known that the overall stiffness of three-pinned members is much less, this is confirmed numerically by *Figures 3–7*. The normal displacement (w[mm]) patterns are quite distinct because of the internal pin, while the precise values have one magnitude difference too around the load application point.

However, the tangential displacements (noted by u, measured in [mm]) of *Figure 4* are just about 3 times greater for the three-pinned setup. These numbers are negligible for three-pinned arches in relation to the normal displacements, but are comparable to the normal displacement values in two-pinned arches.

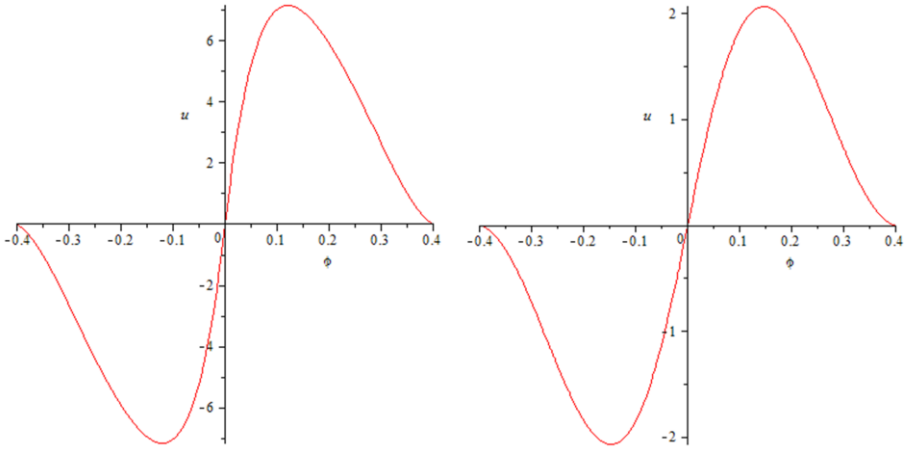

Figure 4. *$\vartheta = 0.4$, (a) three-pinned, (b) two-pinned arch – tangential displacement against the angle coordinate*

The cross-sectional rotations in [rad] of *Figure 5* are less by one magnitude overall in case of two-pins, and furthermore, the two distributions are clearly very distinct. For the two-pinned arch, the rotations are continuous at the crown point and the shape is point symmetric. Meanwhile, for the three-pinned case, there is a discontinuity at the sides of the internal pin. It is also noted that the rotation at the end supports are as well much greater in this later case.

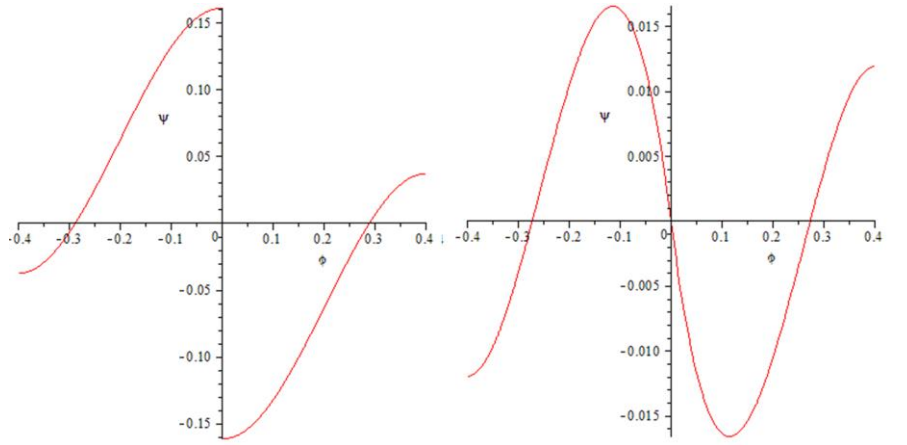

Figure 5. *$\vartheta = 0.4$, (a) three-pinned, (b) two-pinned arch – cross-sectional rotations against the angle coordinate*

The M [Nmm] bending moment distributions (see *Figure 6*) are as well different, with the peak being about 2.5 times greater for three-pins, but the peak rises at different position. It is clearly visible that moment is not transferred between the two parts when there is an internal pin. Further, there is sign change in the moment for two-pinned arches.

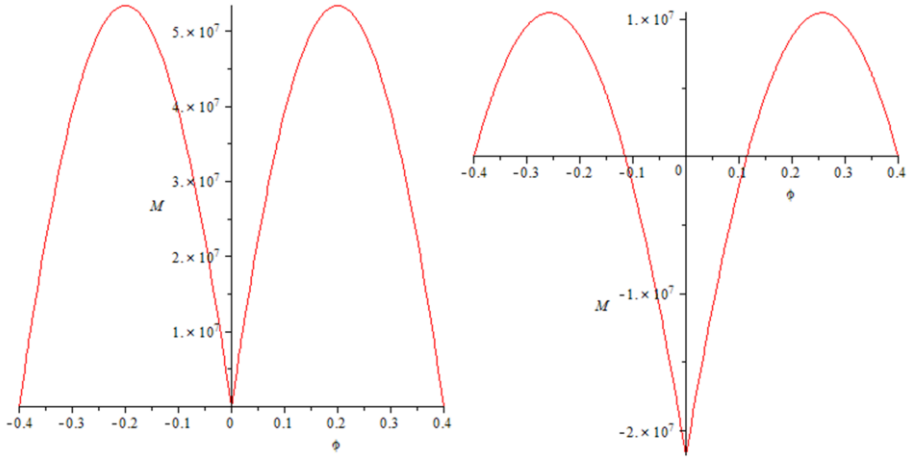

Figure 6. *$\vartheta = 0.4$, (a) three-pinned, (b) two-pinned arch – bending moment against the angle coordinate*

The N [N] axial force level is almost 2 times greater for three-pins as per *Figure 7*. However, it can be concluded that the values do not vary much along the angle coordinate.

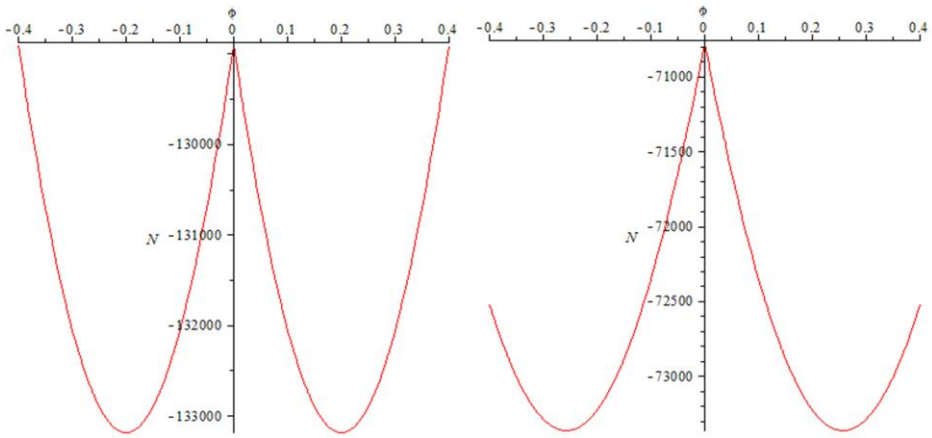

Figure 7. *$\vartheta = 0.4$, (a) three-pinned, (b) two-pinned arch – axial force against the angle coordinate*

3. Conclusions

Two- and three-pinned slender, circular arches were compared within this work to find out the lowest nonlinear buckling loads, displacements and inner forces. The support distance was a fixed value and arches with different angles were placed, starting from very flat (almost straight) to deep arch geometries. It was found that two-pinned arches are stiffer throughout the whole investigated domain,

having much greater buckling loads and less displacement and inner forces when the load levels are identical. At the same time, the pattern of the displacements, rotation and bending moment are distinct between the selected arch types, while the axial force is distributed in a rather similar way along the arc coordinate. The novel model was compared with finite element computations and a good correlation was found.

References

[1] Simitses, G. J. (1976). *An introduction to the elastic stability of structures*. New Jersey: Prentice-Hall. **https://doi.org/10.1115/1.3423874**

[2] Bazant, Z., Cedolin, L. (2010). *Stability of Structures*. World Scientific. **https://doi.org/10.1142/7828**

[3] Gönczi, D., Ecsedi, I. (2022). Thermal stresses in radially non-homogeneous curved beams. *Annals of Faculty of Engineering Hunedoara*, 20 (4), 107–114.

[4] Ecsedi, I., Lengyel, Á. J., Baksa, A., Gönczi, D. (2023). Pure bending of curved beam with non-uniform cross-section. *Multidiszciplináris Tudományok: A Miskolci Egyetem közleménye*, 13 (3), 14–25. **https://doi.org/10.35925/j.multi.2023.3.2**

[5] Dawe, D. J. (1974a). Curved finite elements for the analysis of shallow and deep arches. *Computers & Structures*, 4, 559–580. **https://doi.org/10.1016/0045-7949(74)90007-8**

[6] Dawe, D. J. (1974b). Numerical studies using circular arch finite elements. *Computers & Structures*, 4, 729–740. **https://doi.org/10.1016/0045-7949(74)90041-8**

[7] Gummadi, L. N. B., Palazotto, A. N. (1997). Finite element analysis of arches undergoing large rotations I: Theoretical comparison. *Finite Elements in Analysis and Design*, 24 (4), 213–235. **https://doi.org/10.1016/S0168-874X(96)00051-0**

[8] Palazotto, A. N., Gummadi, L. N. B., Bailey, J. C. (1997). Finite element analysis of arches undergoing large rotations II: Classification. *Finite Elements in Analysis and Design*, 24 (4), 237–252. **https://doi.org/10.1016/S0168-874X(96)00050-9**

[9] Bateni, M., Eslami, M. R. (2014). Non-linear in-plane stability analysis of FGM circular shallow arches under central concentrated force. *International Journal of Non-Linear Mechanics*, 60, 58–69. **https://doi.org/10.1016/j.ijnonlinmec.2014.01.001**

[10] Bradford, M. A., Pi, Y. L., Tin-Loi, F. (2008). Non-linear in-plane buckling of rotationally restrained shallow arches under a central concentrated load. *International Journal of Non-Linear Mechanics*, 43, 1–17. **https://doi.org/10.1016/j.ijnonlinmec.2007.03.013**

[11] Yan, S. T., Shen, X., Chen, Z., Jin, Z. (2017). On buckling of non-uniform shallow arch under a central concentrated load. *International Journal of Mechanical Sciences*, 133, 330–343. **https://doi.org/10.1016/j.ijmecsci.2017.08.046**

[12] Yan, S. T., Shen, X., Chen, Z., Jin, Z. (2018). Collapse behavior of non-uniform shallow arch under a concentrated load for fixed and pinned boundary conditions. *International Journal of Mechanical Sciences*, 137, 46–67. **https://doi.org/10.1016/j.ijmecsci.2018.01.005**

[13] Bradford, M. A., Pi, Y. L., Uy, B. (2002). In-plane stability of arches. *International Journal of Solids and Structures*, 39, 105–125. **https://doi.org/10.1061/(ASCE)0733-9399(2002)128:7(710)**

[14] Karnovky, I. A., Lebed, O. (2021). *Advanced Methods of Structural Analysis*. Cham: Springer. **https://doi.org/10.1007/978-3-030-44394-8**

[15] Pi, Y. L., Bradford, M. A. (2015). In-plane analyses of elastic three-pinned steel arches. *Journal of Structural Engineering*, 141, 06014009. **https://doi.org/10.1061/(ASCE)ST.1943-541X.0001135**

[16] Kiss, L. P. (2024). Stability of arches with internal hinge. *Mathematics and Mechanics of Solids*, 29 (10), 1947–1957. **https://doi.org/10.1177/10812865241245338**

[17] Pi, Y. L., Bradford, M. A. (2014). Effects of nonlinearity and temperature field on in-plane behaviour and buckling of crown-pinned steel arches. *Engineering Structures*, 74, 1–12. **https://doi.org/10.1016/j.engstruct.2014.05.006**

[18] Oliveira, M. M., Rocha Segundo, J. S., Azevedo, I. S., Silveira, R. A. M., Sarmanho, A. M. C., Silva, A. R. D. (2021). Advanced parametric study of three-pinned steel arches. In: *Proceedings of the joint XLII Ibero-Latin-American Congress on Computational Methods in Engineering and III Pan-American Congress on Computational Mechanics*, November 9–12, 2021.

[19] Bradford, M. A., Pi, Y. L. (2015). Geometric nonlinearity and long-term behavior of crown-pinned CFST arches. *Journal of Structural Engineering*, 141 (8), 04014190. **https://doi.org/10.1061/(ASCE)ST.1943-541X.0001163**

[20] Kiss, L. P. (2015). *Vibrations and stability of heterogeneous curved beams*. Ph.D Thesis. Miskolc: Institute of Applied Mechanics, University of Miskolc, Hungary.